COMPARATIVE BEHAVIOUR OF 'I BEAM- RHS COLUMN' JOINTS WITH AND WITHOUT WEB WELD

Miguel A. Serrano-López*[1], Carlos López-Colina[1], Yong C. Wang[2], Miguel Lozano[1], Fernando L. Gayarre[1]

[1] University of Oviedo, Dep. Construction and Manufacturing Engineering, Campus Gijón, 33203 Spain

[2] The University of Manchester, School of Mechanical, Aerospace and Civil Engineering, Manchester M13 9PL, United Kingdom

Abstract

This paper presents the results of an experimental and numerical comparative study for beam-column joints constructed of welding open section beams to rectangular hollow section columns between welding the entire beam profile and welding only the beam flanges. Since flanges of open section beams contribute most to the joint stiffness and moment resistance, welding the flanges only has the potential of achieving nearly the same joint stiffness and moment resistance as welding the entire beam profile while reducing the cost of welding considerably. However, it is necessary to quantify the effects. Furthermore, since the beam web is conventionally considered to resist the beam shear force, it is also necessary to investigate whether premature shear failure will occur in the case of welding the flanges only.

This paper presents the results of 27 tests and accompanying detailed numerical modelling to provide further insight. The tests considered the effects of different welding arrangements, different dimensions and different beam to RHS width ratios. The experimental observations suggest that due to flexibility of the RHS face, the contributions of the beam web weld to the total joint stiffness and moment resistance are much lower than those of the beam web to the beam section. Furthermore, if only the beam flanges are welded, the flange welds have much higher shear resistances than would be applied in realistic applications.

Based on these findings, the characteristics of welded open section beam to RHS column joints can be quantified by using the contributions of the beam flanges only.

Keywords:

Beam-column joints, Tubular structures, Numerical simulation, Welded joints

* Corresponding author. Tel.: +34-985181947; fax: +34-985182433.
E-mail address: serrano@uniovi.es (Miguel A. Serrano-López).

Nomenclature:

RHS	Rectangular hollow section
SHS	Square hollow section
IPE	European profile I shape
F	refers to flanges of the beam
W	refers to web of the beam
b_0	width of the hollow section
h_0	depth of the hollow section
t_0	thickness of the hollow section
A	cross section area of hollow section
b_f	width of the beam flange
h	depth of the beam
t_f	thickness of the beam flange
t_w	thickness of the beam web
β	ratio of widths (b_f/b_0)
f_u	ultimate strength
f_y	yield strength
E	Young's modulus
ε_u	ultimate deformation
a_w	weld throat thickness
L_w	length of weld
β_w	coefficient of reduction for welds
f_{ya}	average yield strength
f_{uf}	ultimate strength from tube face coupons
f_{yf}	yield strength from tube face coupons
LVDT	Linear Variable Differential Transformer
S_{ini}	initial rotational stiffness
S_b	beam stiffness
M_j	moment resistance of the joint
M_b	moment resistance of the beam
V	relative to shear force

1. Introduction

Structural hollow sections are increasingly used in steel building construction as an alternative to traditional open profiles. This is owing to several advantages of tubular

sections for structural applications as described in [1] and [2], including structural efficiency and attractive appearance.

An efficient combination is to use rectangular or square hollow sections (RHS or SHS) as columns and open profiles (IPE) as beams because this construction form takes full advantage of the strengths of both types of sections in terms of their mechanical behaviour – hollow sections and I-sections possessing superior compressive resistance and bending resistances respectively. Connections between these two types of sections can be welded or bolted.

There have been many research studies [3-6] on bolted joints between open steel beam sections and tubular columns, as this form of joint can take advantage of shop preparation and easy erection on site. However, welded joint has the advantage of creating a streamlined “neat” appearance and the potential to develop moment resisting connections. If welding can be easily operated onsite, it can become a viable construction technology. In welded joints, to increase the stiffness and bending moment capacity of the joint, it is common practice to fully weld all around the beam section perimeter on to the front face wall of the tubular column, i.e. around the flanges and the web of the I-beam. However, this requires a large amount of welding, which is not only costly but also can increase the heating input during the welding process thereby resulting in changes in the material properties [7, 8].

In case of an IPE beam, the web height is much larger than the flange width of the beam, yet it is the flanges that contribute most to the bending rigidity and resistance of the beam and the joint. Therefore, not welding the web could drastically reduce the amount of welding, leading to significant cost savings. For example, for the type of joints considered in this research, the savings in weld length would range from 40 to 45%.

When the beam is under bending, not welding the web to the steel tube is unlikely to be detrimental to the joint behaviour, because the initial rotational stiffness and moment resistance of the beam comes primarily from the flanges. In fact, when forming part of a connection to a tubular column, the web of the I-section may contribute even less due to greater flexibility of the tube connected to the web compared to that connected to the flanges. However, there are usually shear forces in beams and the web of an I-section is commonly assumed to provide the required shear resistance. How the shear resistance is provided in a connection without welding the web to the steel tube is a concern.

In order to evaluate the performance of welded I-beam to tubular column joints, the authors have carried out an extensive programme of tests and numerical simulation studies on welded open profile beams to tubular columns with different section sizes and different welding arrangements – full weld around the flanges and the web, weld around the flanges only and weld around the web only.

The objectives of this study are to demonstrate low contribution of the web weld to joint stiffness and resistance and to provide deep insight of the loadbearing mechanisms of welded I-beam to tubular column joints with and without welding the web of the beam. This paper presents the results of a large experimental campaign complemented with numerical analyses to comprehensively examine contributions of the welded web to the initial rotational stiffness and bending moment resistance of the joint, and the shear resistance mechanism, in particular in joints without welding the web.

2. Experiments

The experiment programme consisted of a total of 27 full beam-column joint tests to determine the behaviour of joints with different dimensions under different welding configurations, and material testing to obtain the relevant mechanical properties of steel to be implemented in the numerical model.

2.1 Beam-column joint tests

The joint tests were carried out in cruciform as shown in figure 1. This figure also shows the three different welding configurations: weld around the flanges and the web (to be referred to as F+W weld), weld around the flanges only (to be referred to as F only) and weld around the web (to be referred to as W weld). Table 1 lists the main parameters of the 27 tests. They are grouped in three phases. The twelve joints tested in phase 1 (specimens 1.1 to 1.4) and phase 2 (specimens 2.1 to 3.9) in total consisted of six pairs of joints, the difference in each pair being welding both the flanges and the web of the beam (F+W) or only welding the flanges of the beam (F). Phases 1 and 2 used different RHS section sizes. Within each of these two phases, the beam dimensions were changed, giving different beam depths and two beam width to RHS width ratios (flange width=RHS width (β=1), flange width=0.73 RHS width (β=0.73)). In Phase 3 (specimens 4.1 to 4.15), five different beam-column joint configurations were tested combining two RHS and three IPE sections as described in table 1, and each beam-column joint configuration having all three welding configurations (F+W, F, W). Three beam width to RHS width ratios (β=1, β=0.8 and β=0.73) were considered in phase 3.

Fig. 1. One set of specimens: 4.7 with all the perimeter welded (F+W), 4.8 with only the flanges welded (F) and 4.9 with only the web welded

Table 1. Beam-to-column joint combinations

Specimen ID	Column (h_0xb_0xt_0)	Beam IPE	Ratio b_f/b_0	Weld Throat Thickness (mm) F	W
1.1	150x100x6	200	1.00	4.36	4.01
1.2	150x100x6	200	1.00	4.52	-
1.3	150x100x6	140	0.73	3.86	3.82
1.4	150x100x6	140	0.73	4.05	-
2.1	250x100x6	200	1.00	4.23	4.19
2.2	250x100x6	200	1.00	3.98	-
2.3	250x100x6	140	0.73	3.92	3.77
2.4	250x100x6	140	0.73	4.07	-
3.4	200x150x6	300	1.00	6.20	5.64
3.5	200x150x6	300	1.00	6.43	-
3.8	250x150x6	300	1.00	6.38	5.25
3.9	250x150x6	300	1.00	6.28	-
4.1	150x100x4	200	1.00	5.11	4.06
4.2	150x100x4	200	1.00	4.79	-
4.3	150x100x4	200	1.00	-	3.88
4.4	200x100x4	200	1.00	4.68	3.97
4.5	200x100x4	200	1.00	5.62	-
4.6	200x100x4	200	1.00	-	3.83
4.7	150x100x4	160	0.80	4.43	3.72
4.8	150x100x4	160	0.80	4.47	-
4.9	150x100x4	160	0.80	-	3.72
4.10	200x100x4	160	0.80	3.78	3.66
4.11	200x100x4	160	0.80	4.28	-
4.12	200x100x4	160	0.80	-	3.59
4.13	200x100x4	140	0.73	4.10	3.44
4.14	200x100x4	140	0.73	3.80	-
4.15	200x100x4	140	0.73	-	3.48

(F) Flanges welded. (W) Web welded.

For the specimens with web welding only, it was necessary to cut both flanges of the beam as shown in figure 2, to allow rotation of the beam during the test without the flanges touching the column face. In case of F joints no specific adjustments were considered for the web. Table 2 presents the dimensions of the beam web cutting for different IPE sections.

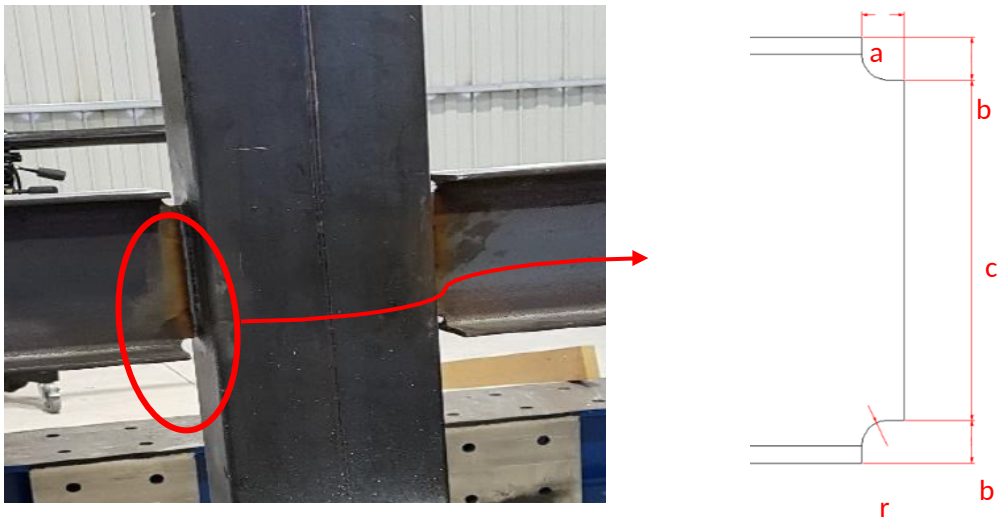

Fig. 2. Details of a web weld only (W) specimen

Table 2. Dimensions of beam cutting for web weld only joints

IPE	a [mm]	b [mm]	c [mm]	r [mm]
200	20.0	14.0	183.0	7.0
160	20.0	11.8	145.2	5.9
140	20.0	11.2	126.2	5.6

Figure 3 shows the experimental set up together with drawings of an adaptable support and a joint specimen. The RHS section was 900 mm in length and the length of the IPE on each side of the RHS was 450 mm. The IPE sections were welded to the middle of the tube so the assembly could be considered to be doubly symmetrical as was proven by the test results to be presented later. The tests were carried out under displacement control at a speed of 4 mm/min in a reaction frame (see figure 3). A hydraulic jack GIB-500 with a load capacity of 500 kN was used to introduce the load as a vertical compression applied on the top of the column. The ends of the beams were simply supported on a pair of adaptable supports that allowed different total spans of the specimens to accommodate the different depths of the tubes. The vertical reactions at the beam end supports produced bending moments in the joints and they were calculated together with the angle of rotation for plotting the joint moment-rotation curves.

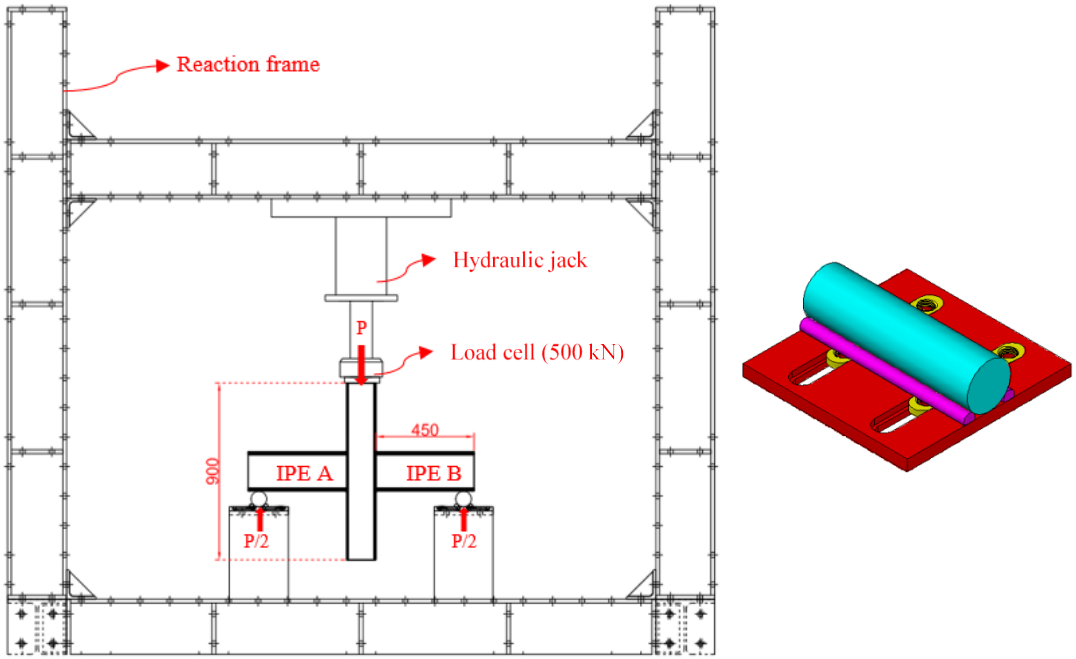

Fig. 3. Experimental set-up and details of adaptable supports

To measure the rotation angle, two different methodologies were followed. For the joints tested in phase 1 (specimens 1.1 to 1.4), software Catman for QuantumX MX1601B and four LVDTs were used. The four LVDTs, as shown in figure 4, were positioned on the middle of the outside part of the beam flanges to indirectly obtain the rotation angle while taking into account the beam's depth, according to the procedure used in [5]. However, some problems were encountered with this method and a different procedure was followed for the other tests. For joints tested in phases 2 and 3, a Digital Image Correlation (DIC) system, [9] [10] was used. A pair of cameras allowed to measure, without contact, 3D displacements (figure 5), that were used to calculate the beam rotation during the tests. The applied load entered by an analogue connector was synchronized with the displacements, allowing easy post-processing of joint moment-rotation relationships.

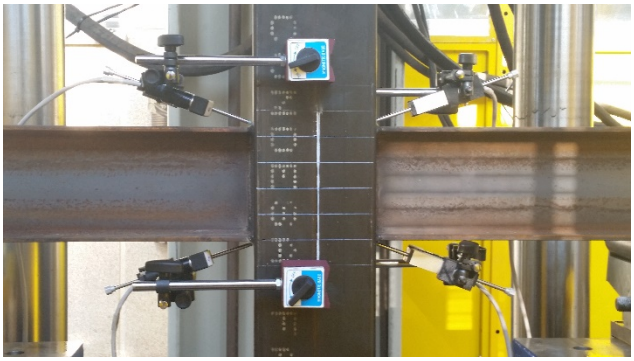

Fig. 4. LVDTs to indirectly obtain the angle of rotation

The DIC equipment used was an Aramis 5M from GOM and the process of images was carried out with compatible software Aramis v6. For this measurement method, it was necessary to prepare the specimens before the tests with a stochastic pattern, called speckle pattern, applied on the specimen surface by spraying. The surface must be free of oil and grease for a correct adhesion of the painting coat. The size of the pattern must be selected to obtain the desired accuracy [11]. For the specimens included in Phase 2, a pair of lens with 23 mm of focal distance were used to obtain images of 30x25 mm size, so only rotation of one of the connections could be registered (figure 5a). Nevertheless, for the fifteen joints tested in phase 3 the focal length of the lens was 12 mm thereby allowing images of a much bigger size (1900x1700 mm) to be acquired, which was adequate to obtain the rotations of both connections simultaneously. The displacements observed in figure 5b demonstrate symmetrical behaviour of the joint as assumed.

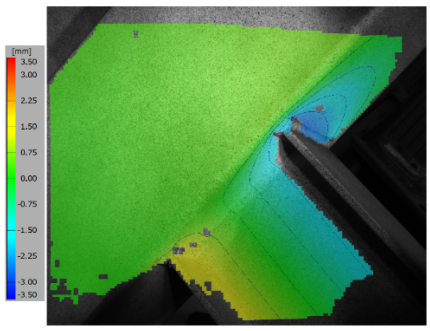

a) Sample of displacements for a joint in phase 2

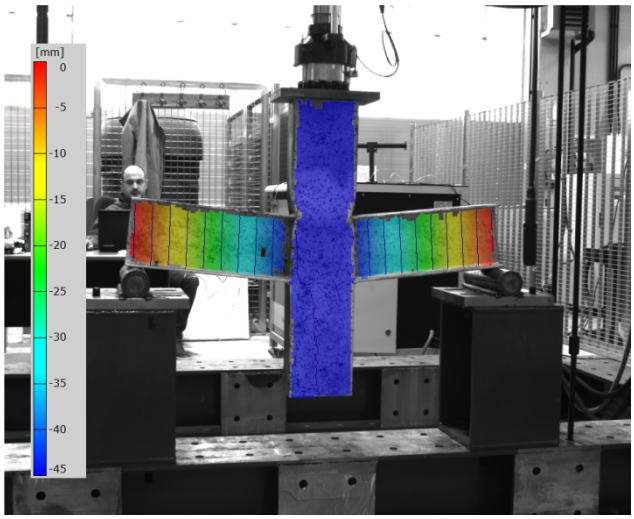

b) Sample of displacements for a joint in phase 3

Fig. 5. 3D displacement measurements with digital image correlation DIC

2.2 Material characterization

All the tubular sections used nominal S275 grade steel and were cold formed welded structural hollow sections [12]. To obtain the mechanical properties of steel of the columns and beams, standard tensile tests [13] were carried out. For each RHS, two coupons were extracted from a frontal face and two more from a lateral face, avoiding the welded wall of the tube. For the IPE sections, two coupons from the flanges and two more from the web were extracted. A total of 28 coupons from the tubular sections

and 20 coupons from the IPE profiles were tested. Coupons were machined according to [13]. These material characterization tests were carried out, under displacement control, in a universal testing machine; model MTS810, with a load cell capacity of 100 kN. During the tests, the strain was measured by means of an extensometer MTS model 634.31F24, and also from the DIC equipment with a 50 mm focal length. Table 3 presents the average measured values of mechanical properties of steel for the columns and beams.

Welds were carried out by using electrode arc welding following appropriate welding procedure specifications (WPS). A basic coated electrode AWS/ASME: A5.1; SFA 5.1 E7018 was used. The electrodes overmatched the base metal strength, later in Section 3 some more details regarding the electrodes are given.

Table 3. Average mechanical properties for RHS and IPEs

Column (h_0xb_0xt_0)	f_y [N/mm^2]	f_u [N/mm^2]	E [GPa]	ε_u [%]
150x100x6	467.5	532.8	201.2	26.22
250x100x6	469.1	558.8	200.4	27.24
200x150x6	397.0	472.8	212.5	28.78
250x150x6	438.3	535.0	203.6	26.41
150x100x4	412.0	477.2	201.9	21.28
200x100x4	393.9	502.1	194.1	25.26
Beam IPE	f_y [N/mm^2]	f_u [N/mm^2]	E [GPa]	ε_u [%]
200(1)	367.5	458.9	199.0	24.64
140(2)	337.0	476.8	198.1	22.72
300	298.5	451.4	207.3	25.40
200(1)	354.1	453.2	202.7	24.01
160	321.2	463.0	200.0	25.08
140(2)	342.7	443.8	207.9	24.82

(1) (2) Different IPE bars

2.3 Experimental results of joint behaviour

The observed failure modes were the same for the same joint with F+W welding of F welding, for both equal-width joints (β =1.0) or different-width joints (β <1.0), as shown in figure 6. For equal-width joints, failure appeared in the lateral walls of the tube in compression. For different-width joints (β <1.0), the frontal face of the tube also experienced a chord face failure. There was no shear failure.

F+W and β =1.0 F and β =1.0 F+W and β <1.0 F and β <1.0

Fig. 6. Failure modes of joints with F+W and F welding with ratios β =1.0 and β <1.0

In order to confirm the assumed symmetrical behaviour of joints, figure 7 compares the measured moment-rotation relationships on the two sides of two joints (tests 4.1 (F+W) and 4.2 (F)). They demonstrate symmetrical behaviour as intended. This indicates that in those tests where measurements were made on only one side of the joint, it is acceptable to use the results as representing the behaviour of both sides of the joint.

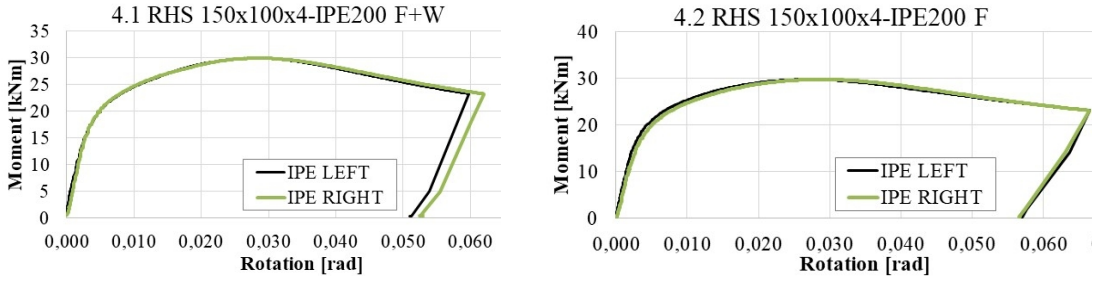

Fig. 7. Symmetrical behaviour of double-side welded joints

Figure 8 compares moment-rotation curves for the phase 3 tests. They indicate that the moment-rotation curves for tests with F and F+W welding were almost identical. The Phase 1 and Phase 2 test results exhibited the same trend. With welding the web only, the moment-rotation response was much more flexible than under F or F+W welding. However, the difference in moments for F and F+W welding at the same rotation is negligible and much lower than that with web weld only. This was unexpected as it would have been assumed that if the flanges and the web were undergoing the same rotation, the moment of the F+W welded joint would be the sum of the moments of the F and W separately welded joints. However, the expected behaviour is based on the assumption of uniform stress in the flanges under bending. The numerical results in Section 3 will show that due to the tube being much stiffer around the corners than in the centre, the flange stress distribution is no longer uniform, with much higher stresses in the flange tips and very low stresses in the middle.

As it was not possible to experimentally measure results to prove this hypothesis, numerical results of stress plots will be used in Section 3 of the paper to demonstrate this effect.

Table 4 lists the rotational stiffness and bending moment resistance of all the tested joints. The initial stiffness of the joint was obtained as the secant stiffness of the linear part of the moment-rotation curve for a rotation corresponding to an indentation of 1/3 of $1\%b_0$, an indentation of $1\%b_0$ being the assumed value for the serviceability deformation limit in joints using RHS [2]. The moment resistance was calculated either at an indentation of $3\%b_0$ or when the maximum moment was reached, whichever occurred first [14].

Table 4. Initial rotational stiffness and moment resistance

Specimen	Weld	Initial stiffness [kNm/rad]	Ratio joint/beam S_{ini}/S_b	Moment resistance [kNm]	Ratio joint/beam M_j/M_b
1.1	F+W			44.1	0.55
1.2	F			42.0	0.53
1.3	F+W			17.8	0.59
1.4	F			17.2	0.57
2.1	F+W	8675.5	8.89	39.7	0.49
2.2	F	9134.9	9.36	30.5	0.38
2.3	F+W	4708.8	12.0	16.9	0.54
2.4	F	2257.6	5.75	15.4	0.52
3.4	F+W	21760.0	7.54	77.4	0.41
3.5	F	20777.0	7.20	85.9	0.46
3.8	F+W	22609.0	7.83	91.8	0.49
3.9	F	22207.0	7.69	93.7	0.50
4.1	F+W	6037.7	6.19	30.0	0.38
4.2	F	6096.3	6.25	29.8	0.37
4.3	W	162.3	0.16	3.1	0.04
4.4	F+W	6019.6	6.17	28.4	0.36
4.5	F	5572.0	5.71	27.8	0.35
4.6	W	158.4	0.16	3.2	0.04
4.7	F+W	2191.2	4.03	12.7	0.32
4.8	F	1501.7	2.76	12.5	0.31
4.9	W	81.5	0.15	1.8	0.04
4.10	F+W	1855.2	3.41	11.2	0.28
4.11	F	1865.3	3.43	11.6	0.29
4.12	W	84.9	0.15	1.9	0.05
4.13	F+W	954.8	2.43	8.9	0.29
4.14	F	965.3	2.46	8.6	0.29
4.15	W	56.1	0.14	1.7	0.05

(F) Flanges welded. (W) Web welded.

The results in table 4 confirm that all the joints with welded flanges (F+W and F) achieved semi-rigid (S_{ini}/S_b=2.43-12.0) and partial strength behaviour (M_j/M_b=0.28-

0.59) according to EN 1993-1-8 [15] definitions, the reference beam stiffness being calculated assuming a beam span to depth ratio of 20. Joints with only the web welded (W) exhibited, as expected, very low stiffness and low bending resistance, with the rotational stiffness and moment resistance ranging from 2.5% to 5.5% and 10%-17% of the initial stiffness and bending moment resistance of the corresponding joints with welded flanges.

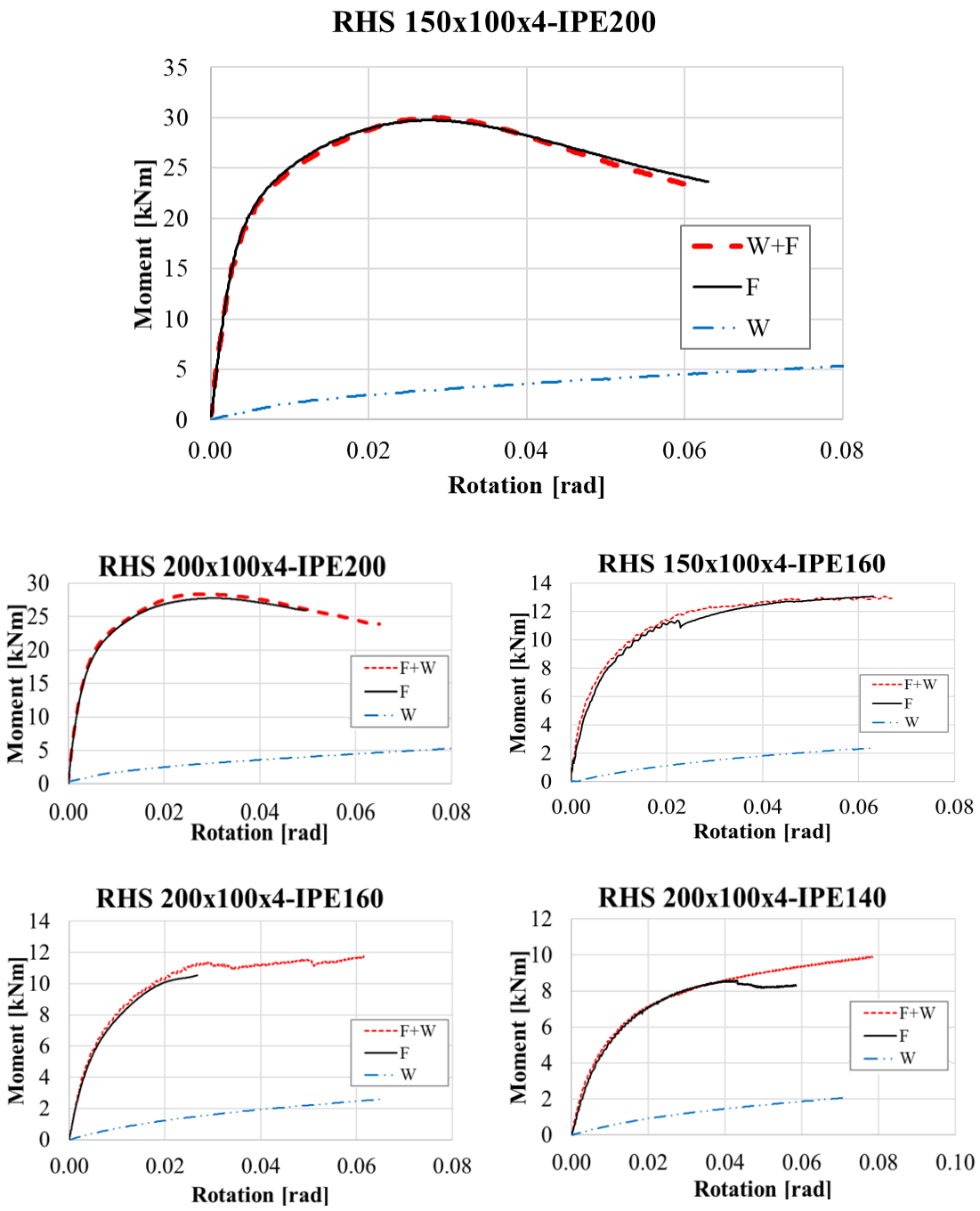

Fig. 8. Comparison of moment-rotation curves for Phase 3 tests

In design of steel beams according to EN 1993-1-1 [16], it is assumed that the web resists shear. As the beam web was not welded in the joints with F weld only, the shear resistance according to EN 1993-1-1 [16] would be negligible and shear failure would govern. However, no isolated shear failure was observed in the F weld joints. The only evidence of any shear failure was partial failure in the welds in the tension zone, which caused the moment-rotation curve to experience a small sudden reduction in bending moment as shown in figure 8. However, the moment-rotation curve continued to increase afterwards and would reach the same bending resistance as the F+W weld joint.

This suggests that the shear force of the beam in the F weld joints was resisted by the flange welds. Table 5 compares the calculated shear resistances of the flange welds with the applied shear force when the failure load is reached. It confirms that although the shear resistances of F weld only joints, obtained by the EC3 1-8 [15], were about 25% lower than those of F+W weld joints, both weld conditions had far greater shear resistance than the applied shear force. In fact, the ratios of test shear force to weld shear resistance of the F weld only joints were all much lower than 0.5, so the applied shear force can be considered low. In addition, it must be taken into account that due to the test configuration with a small lever arm, the applied shear is considerably higher than the usual one in buildings and, even so, the shear is not determinant in the strength of the joint.

Table 5. Shear resistances of welds in F specimens - comparison with the maximum applied shear force

Specimen	a_w	$V_{ult.weld}$[kN]	V_{test}[kN]	$V_{test}/V_{ult.weld}$
1.2	4.52	523.65	101.94	0.19
1.4	4.05	343.10	41.75	0.12
2.2	3.98	463.36	63.81	0.14
2.4	4.07	344.10	32.29	0.09
3.5	6.43	1105.63	185.30	0.17
3.9	6.28	1080.55	198.31	0.18
4.2	4.79	554.38	73.04	0.13
4.5	5.62	649.80	59.78	0.09
4.8	4.47	421.33	30.64	0.07
4.11	4.28	408.31	26.11	0.06
4.14	3.80	325.62	18.53	0.06

The shear resistance of the flange welds was calculated using the following equation, derived from the general failure criteria for fillet weld design [15]:

$$V_{ult.weld} = 2\sqrt{2}\, a_w\, L_w \frac{f_u}{1.25\, \beta_w} \qquad (1)$$

where a_w is the weld throat thickness whose values are listed in table 5.

In summary, the test results have confirmed that joints with F and F+W welds had almost identical moment-rotation behaviour, both achieving semi-rigid and partial strength behaviour. The welds in F weld only joints had sufficient shear resistance. The numerical modelling results in Section 3 will provide further explanations of the experimental observations.

3. Numerical modelling

The joints under consideration have been simulated by means of the FEA software ANSYS 17.0 using shell 181 elements located at the middle surface of the tube walls, and flanges and webs of the beams. The shell element thickness for welds was taken to be the same as the throat thickness a_w of the corresponding weld. Figure 9 shows typical finite element meshes for F+W and F welding conditions. For similar joints these types of elements and fillet weld model were calibrated and validated [17] and were demonstrated to give good results and efficient computation time. In addition, in the F models there was a 3 mm gap between the beam web and the front face of the hollow section to avoid nodes merging or some contact interaction.

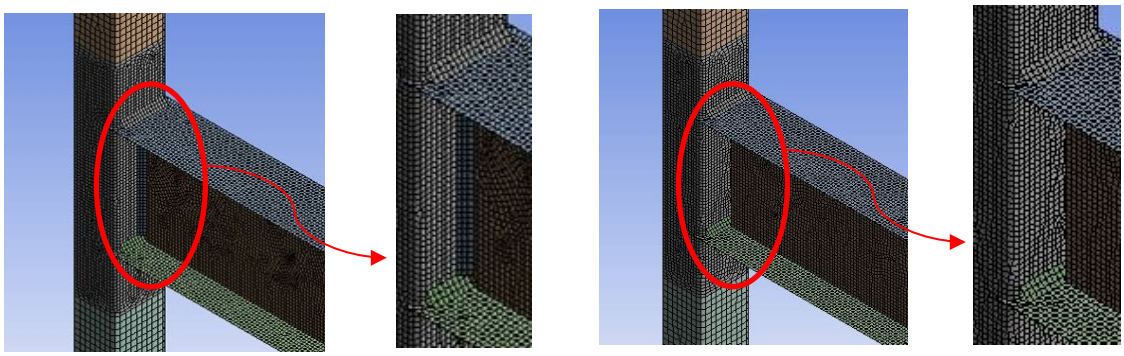

Fig. 9. Finite Element meshes for F+W (left) and F (right)

For the steel tubes, the stress-strain curve was assumed to be elastic-plastic, with a linear strain hardening part that has a slope of E/100 in the plastic zone of the curve, [18] where E is the Young's modulus of steel (see table 3). If the hardening stiffness is obtained from experimental yield and ultimate points it leads to values of about E/200. However, this would underestimate the actual behaviour in the most important part of the stress-strain curve after yielding. Therefore, it was decided to follow the EC3 recommendations for the RHS, also proposed by some other authors [19, 20]. In case

of the open profiles used as beams the adopted hardening stiffness was E/10000 [18], since their material presents a clear yield plateau.

The Eurocode [21] proposal for characterization of cold-formed tubes was used in the finite element analysis. The code uses the base material strengths (f_{yb} , f_{ub}) to calculate the average yield limit (f_{ya}). Nevertheless, in [12] it is considered that coupons extracted from the faces of the RHS, after manufacturing, can be used to calculate the average yield limit $f_{ya,}$ from RHS face properties (f_{yf} , f_{uf}) (table 6). This necessitated using the properties for cold-formed tube in Eurocode 1.3, which is as shown in Equation 2. The accuracy of the results provided by Equation 2 were demonstrated in [22].

$$f_{ya} = f_{yf} + \left(28\,\frac{t_0^2}{A}\right)(f_{uf} - f_{yf}) \qquad (2)$$

Table 6. Calculated average yield limit for RHS

Column (h_0xb_0xt_0)	f_{yf} [N/mm^2]	f_{uf} [N/mm^2]	f_{ya} [N/mm^2]
150x100x6	467.5	532.8	491.3
250x100x6	469.1	558.8	491.9
200x150x6	397.0	472.8	416.3
250x150x6	438.3	535.0	459.7
150x100x4	412.0	477.2	427.5
200x100x4	393.9	502.1	415.1

For welds, comments regarding the mechanical properties in the heat-affected zone [23] where considered. The nominal yield limit and ultimate strength values provided by the electrode manufacturer were used, being f_y=500 MPa and f_u=570 MPa respectively. Symmetry in the geometrical models was taken advantage of to save computation time. Displacement control was adopted on top of the column to simulate the applied load while the vertical displacement of the beam ends was restricted.

To validate the developed numerical model, the results from tests and modelling have been compared. Figure10 shows a selection of the comparison for joint moment-rotation curves, these joints representing different types of welds (F+W, F) and different flange width to tube width ratios (β=1 and β<1). In all of them excellent agreement can be observed, with both set of curves almost identical. As the tube wall was laterally loaded, it was not necessary to include initial imperfection of the RHS tubes, as confirmed in [24] by the authors.

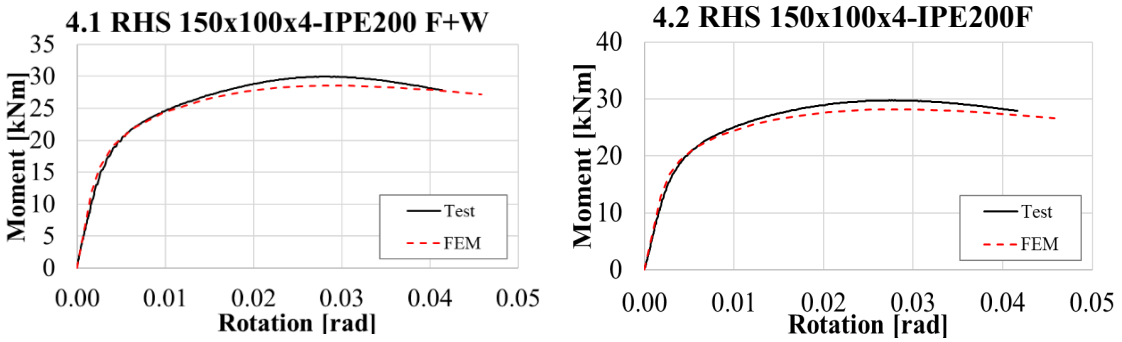

a) Comparison of test *vs.* FE modelling for joints RHS 150x100x4-IPE 200 (β=1)

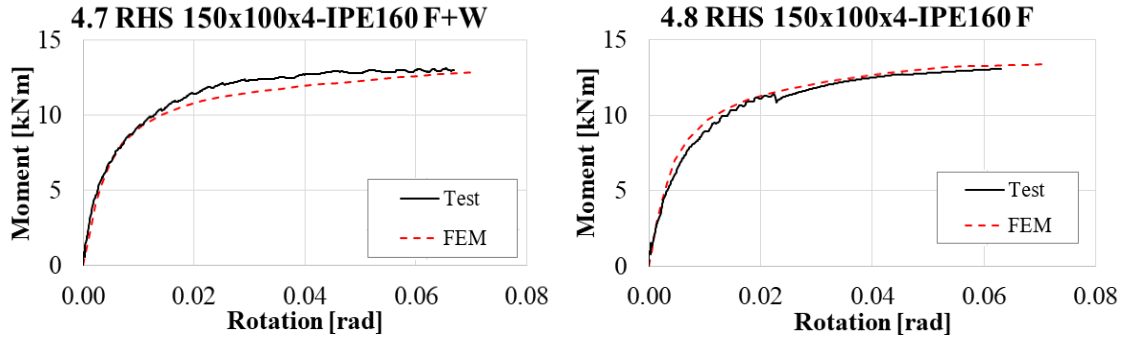

b) Comparison of test *vs.* FE modelling for joints RHS 150x100x4-IPE 160 (β=0.8)

Fig. 10. Comparison of moment-rotation curves for validation of FE modelling

To show overall comparison for all the tests, figures 11 and 12 compare the simulation and test results for the joint initial rotational stiffness and maximum moment capacity respectively for all the joints. Both figures show again good agreement.

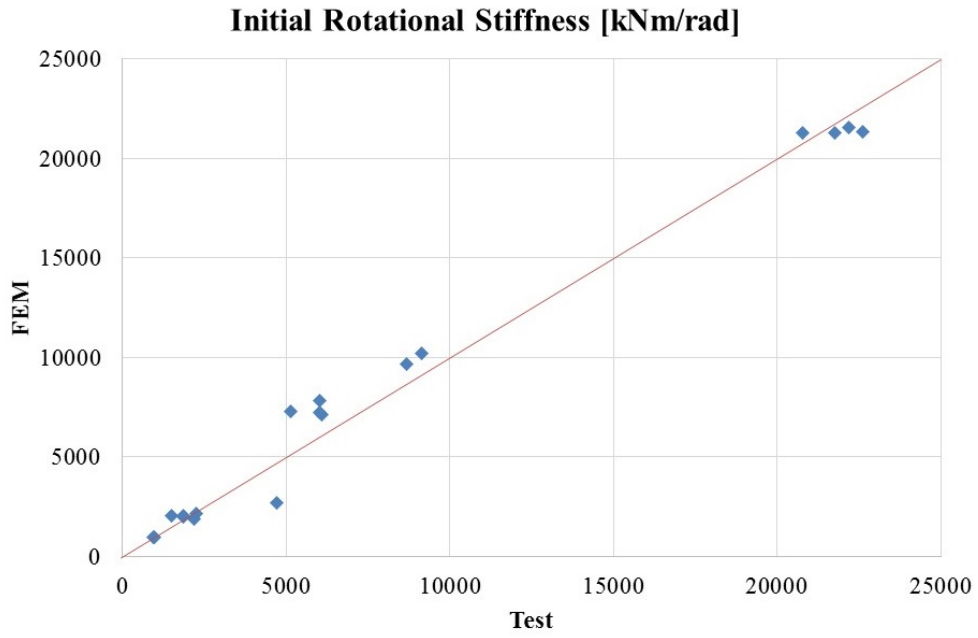

Fig. 11. Comparison between simulation and test results for joint initial rotational stiffness

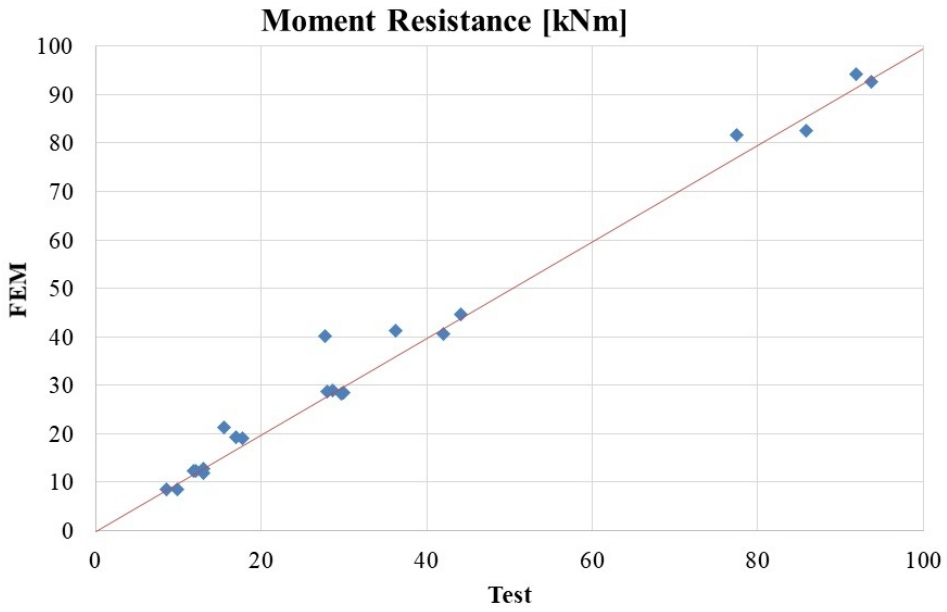

Fig. 12. Comparison between simulation and test results for joint moment resistance

Figure 13 shows a comparison of failure mode between test observation from the DIC equipment and numerical modelling. The same displacement pattern can be seen.

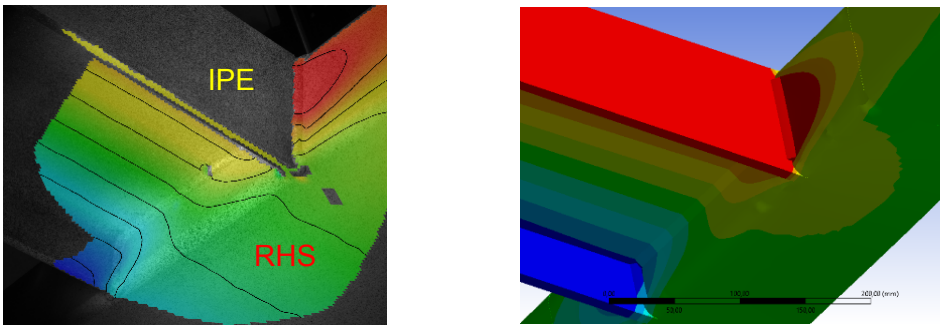

Fig. 13. Comparison of displacement pattern and failure mode between DIC image from test and numerical modelling

The validated numerical models were also used to explain why joints with F+W weld had almost identical moment-rotation curves as the joints with F weld only when other arrangements were kept the same. This was attributed to the flexibility of the tube face connected to the web. To prove this, three hypothetical joints, with F+W, F and W weld, connecting an IPE160 beam to a tube with very high tube stiffness ($E \cong \infty$) were simulated. Figure 14 shows the individual moment-rotation curves of these three joints and the sum of the moment-rotation curves of the joints with F and W weld. The sum of moment-rotation curves of F and W joints is almost identical with the moment-rotation

curve of the F+W joint. This exercise proves that in this case of a rigid tube the joint behaviour with F+W weld is the sum of those with F and W weld, as expected.

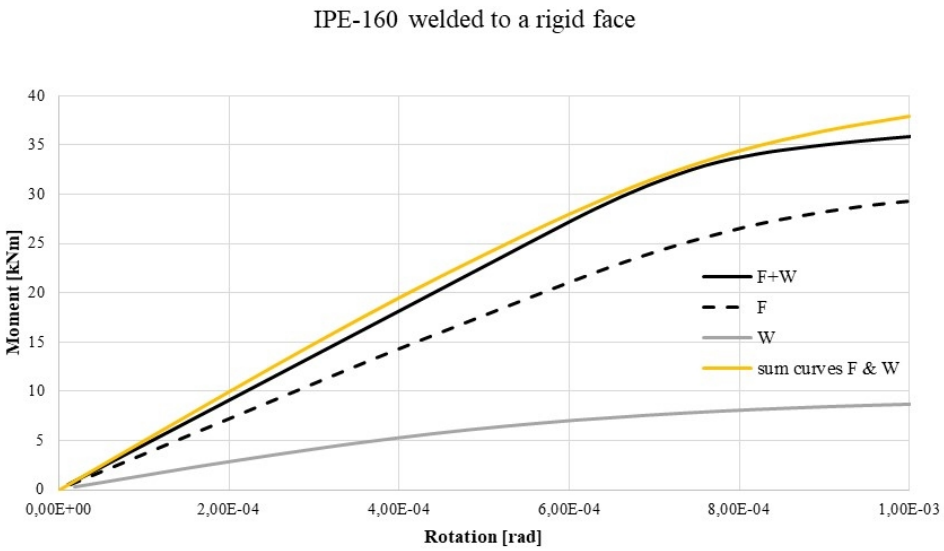

Fig. 14. Simulated moment-rotation curves for a rigid tube connected to IPE160 beam, comparison between F+W joint with sum of F and W joints

Figure 15 further compares the longitudinal stress distributions in the flanges of the beam between F+W and F weld joints. They show uniform stress distribution across the width of the flange in both cases, according to the assumption of plane remaining plane corresponding to the case of an infinitely stiff column face as above mentioned.

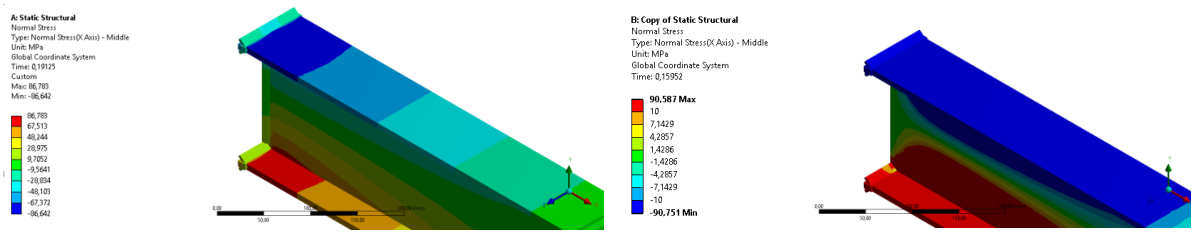

Fig. 15. Normal stress distributions in the flanges of the beam with F+W weld (left) and with F weld (right) when connected to a rigid column face

However, in the case of the tested steel tubes, the much higher rigidity of the tube around the corners attracts stress and strain in the flanges near the tips, with very little stress in the middle (figure 16). Consequently, there is little normal stress in the web of the joint with F+W weld. Under this circumstance, the central part of the tube face, to which the web is connected, may be considered to be ineffective, and this makes the joint with F+W weld behave in almost the identical way as the joint with F weld only.

Some distance away from the weld, the beam flange stress becomes uniformly distributed as assumed in bending behaviour of the beam.

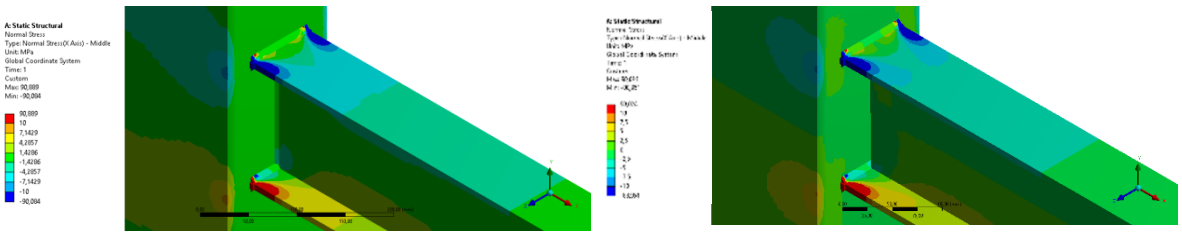

Fig. 16. Normal stress distributions in the flanges of the beam with F+W weld (left) and with F weld (right)

4. Effects of tube width to thickness ratio

The test results indicate that for the tube dimensions used in the tests, the joint stiffness of W weld only joints is small compared to F and F+W weld joints. However, this may be due to the thin steel tubes used in the tests. Also, the test results showed almost identical behaviour between F weld and F+W weld joints, and the explanation for this was the flexibility of the tube section, against due to the thin steel tubes used in the tests. Therefore, it is necessary to investigate whether these conclusions hold when increasing the tube wall thickness.

A series of numerical simulations were performed to investigate the contribution of the web weld to joint behaviour. Four different IPE sections for the beam were considered: IPE160, IPE200, IPE240 and IPE300. Each beam was connected to RHS columns of different sizes with a constant width b_0 but a depth ranging from 100mm to 300mm. The tube wall thickness changed from 4 mm to 12 mm. For IPE160 beams, two tube widths were considered to give two different tube width ratios β. A comparison was made for the joint initial stiffness and moment resistance between F+W weld and F weld.

Table 7 compares initial rotational stiffness values. As expected, the joint initial rotational stiffness increases with the wall thickness. With increasing tube wall thickness, the difference in joint initial rotational stiffness between F+W weld and F weld joints also increases. However, this difference does not exceed 3.5%.

The same conclusion can be applied to the joint moment resistance, as compared in table 8.

Therefore, when quantifying the moment-rotation behaviour of welded beam to RHS/SHS steel tube joints, the joint may be considered to consist of two components only, the upper and lower flanges. Contribution of the web component can be safely neglected without any loss of accuracy.

Table 7. Comparison of simulation results of initial rotational stiffness between F+W and F weld joints

Joint	h_0 [mm]	t_0 [mm]	$2\gamma=b_0/t_0$	$S_{ini(F+W)}$ [kNm/rad]	$S_{ini(F)}$ [kNm/rad]	Difference [%]
RHS (h_0x100xt_0) + IPE 160 8.0=β	100	4	25	2050	2067	-0.79
		8	12.5	4303	4319	-0.36
		12	8.33	6721	6545	2.61
	200	4	25	1982	1994	-0.62
		8	12.5	4111	4122	-0.26
		12	8.33	6380	6224	2.44
	300	4	25	1970	1981	-0.54
		8	12.5	4085	4092	-0.18
		12	8.33	6351	6188	2.57
RHS (h_0x120xt_0) + IPE 160 66.0=β	100	4	30	668	667	0.24
		8	15	3136	3148	-0.39
		12	10	6002	6008	-0,08
	200	4	30	650	648	0.19
		8	15	3007	3019	-0.40
		12	10	5695	5707	-0.21
	300	4	30	653	651	0.20
		8	15	3003	3015	-0.38
		12	10	5674	5685	-0.19
RHS (h_0x100xt_0) + IPE 200 0.1=β	100	4	25	7682	7629	0.68
		8	12.5	15206	15128	0.51
		12	8.33	23195	22813	1.49
	200	4	25	7171	7143	0.38
		8	12.5	13760	13707	0.38
		12	8.33	20777	20507	1.30
	300	4	25	6994	6893	1.45
		8	12.5	13198	13111	0.66
		12	8.33	19953	19711	1.21
RHS (h_0x120xt_0) + IPE 240 0.1=β	100	4	30	10145	10146	-0.01
		8	15	21911	21854	0.25
		12	10	32658	32303	1.08
	200	4	30	9649	9616	0.33
		8	15	19926	19846	0.40
		12	10	29128	28894	0.80
	300	4	30	9345	9440	-1.01
		8	15	19075	19003	0.37
		12	10	27847	27653	0.70
RHS (h_0x150xt_0) + IPE 300 0.1=β	100	4	37.5	14358	14318	0.27
		8	18.7	32673	32615	0.17
		12	12.5	49198	47874	2.69
	200	4	37.5	13747	13970	-1.62
		8	18.7	29986	29957	0.09
		12	12.5	44162	42700	3.30
	300	4	37.5	13401	13404	-0.02
		8	18.7	28761	28732	0.10
		12	12.5	41952	40863	2.59

Table 8. Comparison of simulation results of moment resistance between F+W and F weld joints

Joint	h_0 [mm]	t_0 [mm]	$2\gamma=b_0/t_0$	$M_{(F+W)}$ [kNm]	$M_{(F)}$ [kNm]	Difference [%]
		4	25	9.66	9.55	1.16

RHS (h_0x100xt_0) + IPE 160 $\beta=8.0$	100	8	12.5	23.37	23.10	1.18
		12	8.33	36.06	33.75	6.41
	200	4	25	9.92	9.84	0.85
		8	12.5	23.99	23.65	1.42
		12	8.33	36.74	33.93	7.63
	300	4	25	10.01	9.93	0.82
		8	12.5	24.15	23.79	1.47
		12	8.33	36.88	34.02	7.75
RHS (h_0x120xt_0) + IPE 160 $\beta=6.6$	100	4	30	5.87	5.84	0.43
		8	15	21.14	21.01	0.60
		12	10	36.88	35.59	3.51
	200	4	30	5.95	5.92	0.49
		8	15	21.68	21.52	0.70
		12	10	37.68	35.98	4.53
	300	4	30	6.00	5.96	0.54
		8	15	21.83	21.67	0.73
		12	10	37.85	36.09	4.67
RHS (h_0x100xt_0) + IPE 200 $\beta=0.1$	100	4	25	16,52	16,10	1.95
		8	12.5	39,46	37.92	3.90
		12	8.33	61,99	54.66	11.82
	200	4	25	16,73	16,41	0.67
		8	12.5	40,3	38.60	4.22
		12	8.33	63,34	54.99	13.18
	300	4	25	16,97	16,44	2.20
		8	12.5	40,46	38.65	4.47
		12	8.33	63,61	55.07	13.43
RHS (h_0x120xt_0) + IPE 240 $\beta=0.1$	100	4	30	21.06	20.36	3.32
		8	15	52.86	50.88	3.75
		12	10	85.40	77.46	9.30
	200	4	30	21.69	21.03	3.04
		8	15	54.26	52.34	3.54
		12	10	87.70	78.70	10.26
	300	4	30	21.18	21.10	0.38
		8	15	54.47	52.55	3.52
		12	10	85.32	78.89	7.54
RHS (h_0x150xt_0) + IPE 300 $\beta=0.1$	100	4	37.5	26.45	26.64	0.71
		8	18.7	69.10	69.27	0.24
		12	12.5	108.32	119.18	9.11
	200	4	37.5	27.17	27.21	0.15
		8	18.7	71.71	74.83	4.17
		12	12.5	110.81	123.21	10.06
	300	4	37.5	27.74	27.86	0.43
		8	18.7	72.14	72.40	0.36
		12	12.5	111.19	124.25	10.51

5. Conclusions

This paper has presented the results of an extensive experimental program, finite element modelling and validation against the test results, and a parametric study using the validated model to further examine the behaviour of welded joints between IPE beams and RHS columns. The main aim of the research was to compare the behaviour of joints with welding around the entire beam profile (F+W weld) and welding the beam

flanges only (F weld). The experimental work consisted of 27 full beam-column joints and 40 tensile tests on standardized coupons. The numerical model was developed using the general purpose finite element software ANSYS. The main conclusions of this research are:

1.The test results demonstrated as expected symmetrical behaviour referred to both left and right beams.

2.Also, the digital image correlation equipment was successful in obtaining displacement data of the whole joint without any contact with the test specimen.

3.Using shell elements replicated very well the test results, for joint moment-rotation curves, joint deformation pattern and failure mode.

4.In joints with flange weld only, there was no shear failure because the flange welds had much greater shear resistance than the applied shear force.

5.The contribution of the beam web to the rotational stiffness and moment resistance of welded joints is negligible according to both experimental and the numerical results. The joint moment-rotation curve with full flange and web welding was almost identical to that with welding the flanges only. The difference between these two curves was much lower than the moment-rotation curve of the joint with web weld only.

6.The above results can be explained by the negligibly low stiffness of the RHS face compared to the RHS corners.

7.Further numerical simulations for different joint dimensions, in particular, realistic RHS width to thickness ratios, confirm that the experimental observations can be extended to joints with thick RHS walls (low width to thickness ratios).

8.When developing analytical methods to quantify moment-rotation responses of welded joints between open section beams and RHS columns, the contribution of the web can be safely neglected without losing any accuracy.

This paper is presenting part of the research work carried out in the CIDECT project 5CE [25]. Some others points of this type of joints regarding the component characterization and the corresponding analytical models are also expected to be published.

Acknowledgements

The authors would like to acknowledge the financial support provided by the Spanish Ministry of Economy and Competitiveness through project BIA2017-83467-P and by the CIDECT through project 5CE. They would also like to thank the IEMES Research

Group from the University of Oviedo for their support. Besides, they would also like to thank Swanson Analysis Inc. for their assistance with the use of ANSYS University program.

References

[1] Edkhout M. Tubular Structures in Architecture. CIDECT. Geneva and TU Delft. 2011.

[2] Wardenier J, Packer JA, Zhao XL and Van der Vegte GJ. Hollow sections in structural applications. 2nd Ed. CIDECT. Geneva. 2010.

[3] Elghazouli AY, Málaga-Chuquitaype C, Castro JM, Orton AH. Experimental monotonic and cyclic behaviour of blind-bolted angle connections. Engineering Structures; 31, 2540-2553. 2009.

[4] Málaga-Chuquitaype C, Elghazouli AY, Behaviour of combined channel/angle connections to tubular columns under monotonic and cyclic loading. Engineering Structures; 32, 1600-1616. 2010.

[5] Wang YC, Xue L. Experimental study of moment-rotation characteristics of reverse channel connections to tubular columns. Journal of Construction Steel Research; 85, 92-104. 2013.

[6] Thai HT, Uy B. Rotational stiffness and moment resistance of bolted end plate joints with hollow or CFST columns. Journal of Constructional Steel Research; 126, 139-152. 2016.

[7] Gery D, Long H, Maropoulos P. Effects of welding speed. energy input and heat source distribution on temperature variations in butt joint welding. Journal of Materials Processing Technology; 167, 393-401. 2005.

[8] Linnert GE. Welding Metallurgy. Technology. Vol. 2, 3rd Ed. American Welding Society. Miami. Florida. USA 1967.

[9] Sutton MA, McNeill SR, Helm JD and Chao YJ. Advances in two-dimensional and three-dimensional computer vision. Topics in Applied Physics, 1st ed., PK Rastogi, ed., Springer, Berlin 323–372. 2000.

[10] Schmidt T, Tyson J, Galanulis K. Full-Field Dynamic Displacement and Strain Measurement Using Advanced 3D Image Correlation Photogrammetry. part I. Exp Tech 27(3): 47–50. 2003.

[11] Pan B, Xie H, Wang Z, Qian K and Wang Z. Study on subset size selection in digital image correlation for speckle patterns. Optics Express. 16-10. Optical Society of America. 2008

[12] BS EN 10219-2:2006. Cold Formed Welded Structural Hollow Sections of Non-Alloy and Fine Grain Steels—Part 2: Tolerances, Dimensions and Sectional Properties. 2006.

[13] BS-EN ISO 6892-1:2016. Metallic materials - Tensile testing - Part 1: Method of test at room temperature. 2016.

[14] Zhao X.-L. Deformation limit and ultimate strength of welded T-joints in cold-formed RHS sections. Journal of Constructional Steel Research; 53, 2. 149–165. 2000.

[15] CEN EN-1993-1-8. European Committee for Standardization. Eurocode 3: Design of steel structures. Part 1-8: Design of joints. 2005.

[16] CEN EN-1993-1-1. European Committee for Standardization. Eurocode 3: Design of steel structures. Part 1-1: General rules and rules for buildings. 2005.

[17] Serrano MA, López-Colina C, González J, Gayarre FL. A simplified simulation of welded I beam-to-RHS column joints. International Journal of Steel Structures; 16, 4. 1095-1105. 2016.

[18] CEN EN-1993-1-5. European Committee for Standardization. Eurocode 3: Design of steel structures. Part 1-5: Plated structural elements. 2006.

[19] Yang W, Lin J, Gao N, Yan R. Experimental Study on the Static Behavior of Reinforced Warren Circular Hollow Section (CHS) Tubular Trusses. Applied Sciences; 8 (11). 2237. 2018.

[20] Shao YB, Li T, Lie Seng T, Chiew SP. Hysteretic behaviour of square tubular T-joints with chord reinforcement under axial cyclic loading. Journal of Constructional Steel Research; 67, 1. 140-149. 2011.

[21] CEN EN-1993-1-3. European Committee for Standardization. Eurocode 3: Design of steel structures. Part 1-3: General Rules—Supplementary Rules for Cold-Formed Members and Sheeting. 2006.

[22] López-Colina C, Serrano MA, Lozano M, Gayarre FL, Suárez J. Simplified Models for the Material Characterization of Cold-Formed RHS. Materials; 10(9), paper 1043, doi 10.3390/ma10091043. 2017.

[23] Lozano M, Serrano MA, López-Colina C, Gayarre FL and Suárez J. The influence of the heat-affected zone mechanical properties on the behaviour of the welding in transverse plate-to-tube joints. Materials; 11, paper 266, doi:10.3390/ma11020266. 2018.

[24] Wilkinson T, Hancock G. Predicting the rotation capacity of cold-formed RHS beams using finite element analysis. Journal of Constructional Steel Research; 58, 11. 1455-1471. 2002.

[25] Serrano MA, López-Colina C, Lozano M, López F, Iglesias G. Characterization of 'I Beam-RHS Column' Joints through the Component Method; Report 5CE CIDECT, 2017.